Biliary epithelial injury-induced regenerative response by IL-33 promotes cholangiocarcinogenesis from peribiliary glands

Hayato Nakagawa[a,1,2], Nobumi Suzuki[a,b,1], Yoshihiro Hirata[a], Yohko Hikiba[b], Yoku Hayakawa[a], Hiroto Kinoshita[a], Sozaburo Ihara[a], Koji Uchino[a], Yuji Nishikawa[c], Hideaki Ijichi[a], Motoyuki Otsuka[a], Junichi Arita[d], Yoshihiro Sakamoto[d], Kiyoshi Hasegawa[d], Norihiro Kokudo[d], Keisuke Tateishi[a], and Kazuhiko Koike[a]

[a]Department of Gastroenterology, The University of Tokyo, Bunkyo-ku, Tokyo 113-8655, Japan; [b]Division of Gastroenterology, Institute for Adult Diseases, Asahi Life Foundation, Chuo-ku, Tokyo 103-0002, Japan; [c]Division of Tumor Pathology, Department of Pathology, Asahikawa Medical University, Higashi Asahikawa, Hokkaido 078-8510, Japan; and [d]Hepato-Biliary-Pancreatic Surgery Division, Department of Surgery, The University of Tokyo, Bunkyo-ku, Tokyo 113-8655, Japan

Edited by Jeffrey W. Pollard, Albert Einstein College of Medicine, Bronx, NY, and accepted by Editorial Board Member Tak W. Mak April 7, 2017 (received for review November 24, 2016)

The carcinogenic mechanism of extrahepatic cholangiocarcinoma (ECC) is unclear, due at least in part to the lack of an appropriate mouse model. Because human studies have reported frequent genetic alterations in the Ras- and TGFβ/SMAD-signaling pathways in ECC, mice with tamoxifen-inducible, duct-cell–specific Kras activation and a TGFβ receptor type 2 (TGFβR2) deletion were first generated by crossing *LSL-Kras*^{G12D}, *Tgfbr2*$^{flox/flox}$, and *K19*^{CreERT} mice (*KT-K19*^{CreERT}). However, *KT-K19*^{CreERT} mice showed only mild hyperplasia of biliary epithelial cells (BECs) in the extrahepatic bile duct (EHBD) and died within 7 wk, probably a result of lung adenocarcinomas. Next, to analyze the additional effect of E-cadherin loss, *KT-K19*^{CreERT} mice were crossed with *CDH1*$^{flox/flox}$ mice (*KTC-K19*^{CreERT}). Surprisingly, *KTC-K19*^{CreERT} mice exhibited a markedly thickened EHBD wall accompanied by a swollen gallbladder within 4 wk after tamoxifen administration. Histologically, invasive periductal infiltrating-type ECC with lymphatic metastasis was observed. Time-course analysis of EHBD revealed that recombined BECs lining the bile duct lumen detached due to E-cadherin loss, whereas recombined cells could survive in the peribiliary glands (PBGs), which are considered a BEC stem-cell niche. Detached dying BECs released high levels of IL-33, as determined by microarray analysis using biliary organoids, and stimulated inflammation and a regenerative response by PBGs, leading eventually to ECC development. Cell lineage tracing suggested PBGs as the cellular origin of ECC. IL-33 cooperated with Kras and TGFβR2 mutations in the development of ECC, and anti–IL-33 treatment suppressed ECC development significantly. Thus, this mouse model provided insight into the carcinogenic mechanisms, cellular origin, and potential therapeutic targets of ECC.

extrahepatic cholangiocarcinoma | IL-33 | organoid | ILC2 | amphiregulin

Cholangiocarcinoma (CC) is a highly malignant tumor with features of bile duct (BD) epithelial differentiation, the incidence of which is increasing worldwide (1). CC is classified according to anatomical location—intrahepatic and extrahepatic cholangiocarcinoma (ICC and ECC, respectively). ECC is further divided into hilar and distal CC, depending on the insertion site of the cystic duct. Further classification of ICC and ECC is based on tumor morphology: mass-forming (nodular), periductal-infiltrating (sclerosing), and intraductal-growing (papillary) CC (2). Although most CC cases arise sporadically, several risk factors have been established, including primary sclerosing cholangitis (PSC), liver flukes, hepatitis viral infection, hepatolithiasis, and congenital abnormalities of the pancreatic and biliary ducts (1). Most of these conditions create chronic inflammation in the biliary tree and liver; therefore, chronic inflammation plays a key role in CC development. However, the exact mechanism of inflammation-associated cholangiocarcinogenesis is unclear.

Recent next-generation sequencing technology has enabled comprehensive mutational profiling of CC and has shown that the mutational spectrum differs according to anatomical subtype and underlying etiology (3, 4). In the embryonic stage, the extrahepatic bile duct (EHBD) develops from the embryonic hepatic diverticulum, whereas the intrahepatic bile duct (IHBD) originates within the liver from the ductal plate (5). Therefore, the IHBD and EHBD may exhibit distinct properties and different carcinogenetic processes. Although at present, the same chemotherapeutic strategy is used for CC irrespective of the underlying etiology and anatomical subtype, personalized approaches should be explored.

The cellular origin of CC is also a topic of interest. Although CC is considered to originate from biliary epithelial cells (BECs), recent studies have suggested that multiple cell types could develop into CC (6–8). For example, hepatocytes can transdifferentiate into biliary cells through activation of Notch signaling and eventually give rise to ICC (6, 7). With regard to the EHBD, recent anatomical and immunohistochemical (IHC) analyses revealed that peribiliary glands (PBGs), clusters of epithelial cells residing in the submucosal compartment of the EHBD, form epithelial networks within the walls of EHBDs and might function as BEC stem-cell niches. Therefore, PBGs have attracted attention as a candidate for

Significance

Death-driven compensatory proliferation to repair tissue defects is an important promoter of inflammation-associated carcinogenesis. Our work using a mouse model demonstrates that a biliary epithelial injury-induced regenerative response mediated by IL-33 accelerates development of extrahepatic cholangiocarcinoma (ECC) from peribiliary glands, an effect that was suppressed by anti–IL-33 treatment. Thus, IL-33 is a potential therapeutic target for ECC, and the mouse model reported in this study will enable identification of the mechanisms of biliary injury-based carcinogenesis.

Author contributions: H.N. and N.S. designed research; K.K. supervised the entire project; H.N., N.S., Y. Hirata, Y. Hikiba, Y. Hayakawa, H.K., and S.I. performed research; J.A., Y.S., K.H., and N.K. provided clinical samples; H.N., N.S., Y. Hirata, K.U., Y.N., H.I., M.O., J.A., Y.S., K.H., N.K., K.T., and K.K. analyzed data; and H.N. and Y. Hirata wrote the paper.

The authors declare no conflict of interest.

This article is a PNAS Direct Submission. J.W.P. is a guest editor invited by the Editorial Board.

Data deposition: Microarray data were deposited in the Gene Expression Omnibus database (accession no. GSE88900).

[1]H.N. and N.S. contributed equally to this work.

[2]To whom correspondence should be addressed. Email: hanakagawa-tky@umin.ac.jp.

This article contains supporting information online at www.pnas.org/lookup/suppl/doi:10.1073/pnas.1619416114/-/DCSupplemental.

the origin of ECC (9, 10). However, no conclusive evidence is available.

An appropriate mouse model is indispensable for understanding the molecular pathogenesis and identifying the cellular origin of cancer, as well as for exploring new therapeutic targets. Several useful mouse models of ICC have been established recently (6–8, 11, 12). However, because most of these models were generated by liver-specific gene manipulation or application of hepatotoxins, CC was limited to the intrahepatic or perihilar area. The lack of an appropriate mouse model has hampered investigation of ECC carcinogenesis. Therefore, in this study, a mouse model of inflammation-based ECC was established by duct-cell–specific gene manipulation and was used to investigate carcinogenic mechanisms and identify therapeutic targets.

Results

Generation of Mice Exhibiting Duct-Cell–Specific Kras Activation and TGFβ Receptor Type 2 Inactivation. To induce duct-cell–specific gene manipulation, we used *K19^{CreERT}* mice, in which tamoxifen (TAM)-inducible Cre ERT was knocked into the endogenous K19 locus (13). *K19^{CreERT}* mice were crossed with *Rosa26-Lox-Stop-Lox(LSL)-LacZ* reporter mice (*LacZ-K19^{CreERT}*), and oral administration of 200 mg/kg TAM for 3 consecutive days was confirmed to induce efficient gene recombination (~40%) in all parts of the biliary tree, including the EHBD, PBGs, gallbladder (GB), perihilar BD, and IHBD, on day 7 (Fig. S1*A*). Because recent human studies have reported frequent genetic alterations of Ras and TGFβ/SMAD-signaling pathways in ICC and ECC (4), mice exhibiting duct-cell–specific Kras activation and TGFβ receptor type 2 (TGFβR2) inactivation were generated by crossing *LSL-Kras^{G12D}*, *Tgfbr2$^{flox/flox}$*, and *K19^{CreERT}* mice (*KT-K19^{CreERT}*) (14). However, all *KT-K19^{CreERT}* mice died within 7 wk after TAM administration, probably due to respiratory failure caused by lung adenocarcinomas ($n = 15$) (Fig. S1*B*), and only mild hyperplasia of BECs in the EHBD was observed in the biliary tree at this time point (Fig. S1*C*). Thus, additional hits were deemed necessary to induce ECC in vivo.

Loss of E-Cadherin in Combination with Mutation of Kras and TGFβR2 Results in the Development of ECC. E-cadherin, encoded by the *CDH1* gene, is an important adhesion molecule whose loss is associated with poor prognosis in various cancers, including ECC (15, 16). We reported previously that liver-specific deletion of E-cadherin significantly promoted liver cancer development in mice (17). Thus, the effect of E-cadherin deletion in addition to Kras activation and TGFβR2 deletion on the biliary tree was analyzed by crossing *KT-K19^{CreERT}* mice with *CDH1$^{flox/flox}$* mice (*KTC-K19^{CreERT}*). Surprisingly, 90% of *KTC-K19^{CreERT}* mice (18/20) exhibited a markedly thickened EHBD wall accompanied by a swollen GB within 4 wk after TAM administration (Fig. 1*A*). In addition, 30% of *KTC-K19^{CreERT}* mice showed apparent jaundice, sometimes accompanied by hepatic atrophy, and serum levels of total bilirubin were significantly elevated compared with those of TAM-administered control Cre-negative *LSL-Kras^{G12D};Tgfbr2$^{flox/flox}$;CDH1$^{flox/flox}$* (*KTC*) mice (Fig. 1*A* and Fig. S2*A*). All *KTC-K19^{CreERT}* mice died within 4 wk after TAM administration, mainly from liver failure or respiratory failure caused by lung adenocarcinomas (Fig. S2 *B* and *C*). Because this EHBD phenotype was more stable in male (10/10, 100%) than in female mice (8/10, 80%), male mice were used in subsequent experiments.

Histologically, moderately differentiated adenocarcinoma cells resembling human ECC expanded along the EHBD wall, and infiltration of adenocarcinoma extended to the intrahepatic hilar area including a large IHBD (Fig. 1*B*). Cancer glands and normal PBGs coexisted in the thickened EHBD tissue, and cancer glands were negative for E-cadherin and frequently positive for the proliferative marker Ki67, unlike normal PBGs (Fig. S2*D*), suggesting that cancer glands spread through the PBG network. Cancer cells were positive for the biliary markers K7 and K19 and positive for phospho-ERK, which was in line with Kras activation (Fig. S2 *E* and *F*). Recombination of the *Tgfbr2* allele in ECC tissue was confirmed by PCR (Fig. S2*G*). Additionally, poorly differentiated adenocarcinomas were observed frequently, and such cells invaded lymphatic vessels, as confirmed by double staining of K19 and the lymphatic marker LYVE-1, and metastasized to regional lymph nodes (Fig. 1*C*). In contrast, the peripheral small IHBD revealed dysplastic changes in cholangiocytes with inflammatory cell infiltration and ductular reaction, but mass-forming peripheral-type ICC, as reported in other mouse models of ICC, did not develop (8, 11) (Fig. 1*D*). *KTC-K19^{CreERT}* mice with biliary obstruction by ECC revealed markedly dilated IHBDs and focal necrosis of the liver parenchyma as seen in a mouse model of common bile duct (CBD) ligation (18) (Fig. 1*D*). Interestingly, the cystic duct showed wall thickening due to adenocarcinoma infiltration, whereas the GB was almost intact (Fig. 1*D*), suggesting that the sensitivity to these mutations differs depending on the location in the biliary tree (Fig. S2*H*). Thus, *KTC-K19^{CreERT}* mice exhibited periductal infiltrating-type ECC with lymphatic metastasis.

To confirm that ECC in *KTC-K19^{CreERT}* mice was not due to infiltration of hilar ICC but originated from the EHBD, *KTC* mice were crossed with *Albumin-Cre* mice (*KTC-Alb^{Cre}*) in which Cre was expressed in hepatocytes and intrahepatic BECs but not in extrahepatic BECs (Fig. S3*A*). *KTC-Alb^{Cre}* mice exhibited hilar CC and dysplastic changes in the peripheral IHBD with inflammation at 8 wk of age, whereas the EHBD was intact until 4 mo of age (Fig. S3 *B* and *C*). Therefore, ECC in *KTC-K19^{CreERT}* mice originated from the EHBD.

We also analyzed the expression of phospho-ERK, SMAD4, and E-cadherin using IHC in 36 surgically resected human ECC samples, and 19.4% (7/36) of patients exhibited a similar expression pattern as that of our mouse model (phospho-ERK–positive, SMAD4-negative, and E-cadherin–negative) (Fig. 1*E*).

Human CC is frequently accompanied by a desmoplastic reaction and inflammatory cell infiltration, which support carcinogenesis through release of humoral factors from cancer-associated fibroblasts and macrophages (1). Masson's trichrome staining showed collagen deposition in the tumor tissue of *KTC-K19^{CreERT}* mice, and IHC analysis of α-smooth muscle actin confirmed the accumulation of fibroblasts (Fig. 1*F*). Many CD45-positive immune cells, including F4/80-positive macrophages, also infiltrated the tumor stroma (Fig. 1*F*). Thus, ECC in *KTC-K19^{CreERT}* mice mimicked the human tumor microenvironment.

Mutations of Kras, TGFβR2, and E-Cadherin Are All Required for ECC Development. The phenotypes of *LSL-Kras^{G12D};CDH1$^{flox/flox}$;K19^{CreERT}* mice (*KC-K19^{CreERT}*) and *Tgfbr2$^{flox/flox}$;CDH1$^{flox/flox}$;K19^{CreERT}* mice (*TC-K19^{CreERT}*) were evaluated ($n = 10$, each). All *KC-K19^{CreERT}* mice died within 15 wk after TAM administration, probably because of lung adenocarcinomas (Fig. S4*A*). At this time point, *KC-K19^{CreERT}* mice revealed dysplastic changes in the hilar and peripheral IHBD with inflammatory cell infiltration, whereas only slightly increased numbers of PBGs with mild inflammation were found in the EHBD (Fig. S4*B*). *TC-K19^{CreERT}* mice also died within 5 mo after TAM administration for unknown reasons and did not develop biliary tumors during their lifetimes (Fig. S4*C*). Moreover, mice with a single genetic manipulation, i.e., *LSL-Kras^{G12D};K19^{CreERT}* mice (*K-K19^{CreERT}*), *Tgfbr2$^{flox/flox}$;K19^{CreERT}* mice (*T-K19^{CreERT}*), and *CDH1$^{flox/flox}$;K19^{CreERT}* mice (*C-K19^{CreERT}*), were monitored for up to 6 mo after TAM administration ($n = 10$, each), but no biliary tumor of any type was observed (Fig. S4*C*). Thus, genetic manipulations of Kras, TGFβR2, and E-cadherin are all required for ECC development.

E-Cadherin–Deleted Biliary Cells Are Lost from the Surface of the EHBD Lumen but Remain in PBGs. Interestingly, in *KTC-K19^{CreERT}* mice, cancer cells extended laterally through the subepithelial

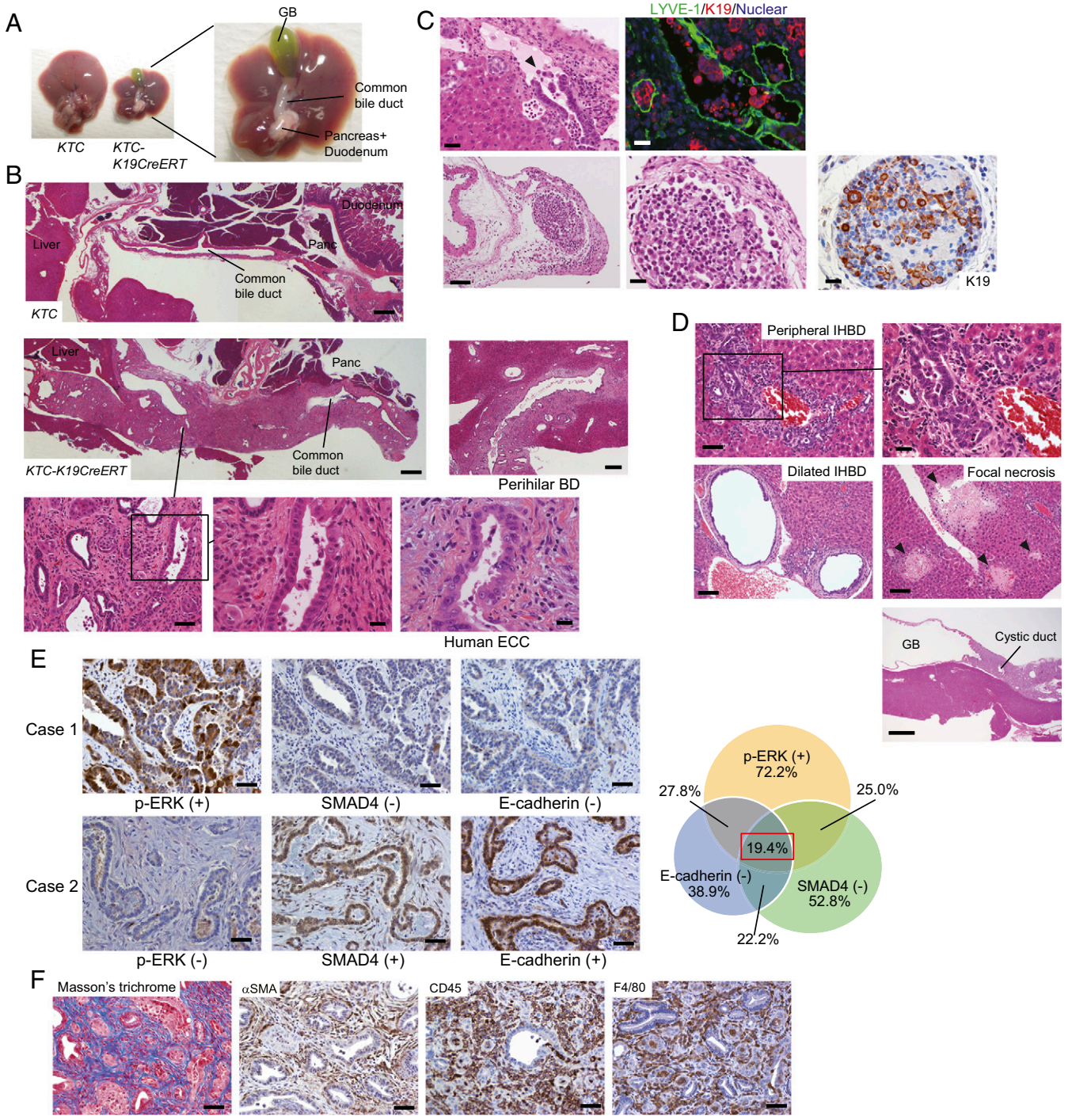

Fig. 1. Loss of E-cadherin in combination with mutation of Kras and TGFβR2 results in the development of ECC. (*A*) Representative images of the liver and bile duct of *KTC* and *KTC-K19*^{CreERT} mice at 3.5 wk after TAM administration. (*B*) H&E-stained images of sagittal sections of the EHBD of *KTC* and *KTC-K19*^{CreERT} mice. (Scale bar: low magnification, 500 μm; middle magnification, 100 μm; high magnification, 20 μm.) H&E-stained images of sagittal sections of the perihilar BD of *KTC-K19*^{CreERT} mice. (Scale bar: 200 μm.) H&E-stained image of human ECC is also shown. (Scale bar: 20 μm.) (*C*) *Upper* panels show invasion by poorly differentiated cancer cells of the lymphatic vessels (*Left*: H&E-staining; *Right*: double IF staining of LYVE-1 and K19). (Scale bar: 20 μm.) *Lower* panels show H&E and IHC images of K19 in regional lymph node metastasis. (Scale bar: *Left* panel, 100 μm; two *Right* panels, 20 μm.) Arrowhead indicates lymphatic invasion by cancer cells. (*D*) H&E-stained images of the peripheral IHBD (scale bar: *Left* panel, 50 μm; *Right* panel, 20 μm), dilated IHBD, focal necrosis of the liver parenchyma (Scale bar: 100 μm), and the GB and cystic duct (Scale bar: 500 μm) of *KTC-K19*^{CreERT} mice. (*E*) IHC analyses of expression of phospho-ERK, SMAD4, and E-cadherin using 36 surgically resected human ECC samples. Representative images of two patients are shown. (Scale bar: 50 μm.) Case 1 exhibits an expression pattern similar to the mouse model. Venn diagram shows the overlap among indicated categories. (*F*) ECC microenvironment in *KTC-K19*^{CreERT} mice. (*Left*) Masson's trichrome staining. The other panels show IHC analyses of the indicated proteins. (Scale bar: 50 μm.)

connective tissue of the EHBD, whereas most surface BECs lining the EHBD lumen were intact (Fig. 2*A*). In fact, IHC analysis of E-cadherin revealed that E-cadherin–deleted BECs were no longer present among surface BECs at 3.5 wk after TAM administration (Fig. 2*B*). Of note, in *C-K19*^{CreERT} and *KC-K19*^{CreERT} mice, E-cadherin–deleted cells were not present

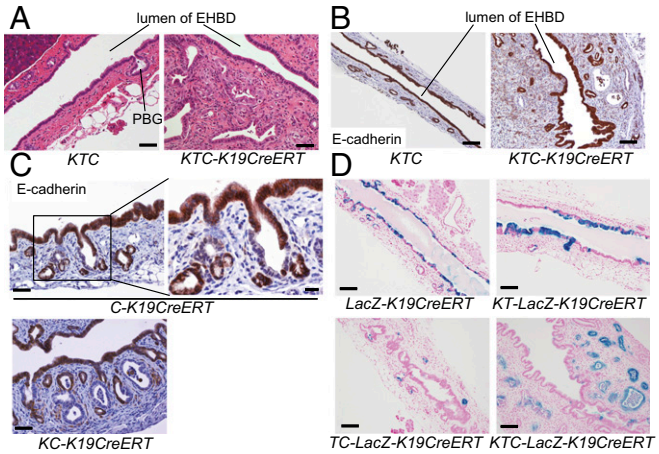

Fig. 2. E-cadherin–deleted biliary cells are lost from the luminal surface of the EHBD but remain in PBGs. H&E staining (*A*) and IHC of E-cadherin (*B*) in the EHBD in *KTC* and *KTC-K19^{CreERT}* mice at 3.5 wk after TAM administration. (Scale bar: *A*, 50 μm; *B*, 100 μm.) (*C*) IHC analysis of E-cadherin in the EHBD of *C-K19^{CreERT}* and *KC-K19^{CreERT}* mice at 3.5 wk after TAM administration. (Scale bar: *Left* panels, 50 μm; *Right* panel, 20 μm.) (*D*) LacZ-stained image of the EHBD from the indicated mice at 3.5 wk after TAM administration. (Scale bar: 100 μm.)

among the surface BECs of the EHBD but were detected in the PBGs at 3.5 wk after TAM administration (Fig. 2*C*). Furthermore, *Rosa26-LSL-LacZ* mice were crossed with *KTC-K19^{CreERT}* mice (*KTC-LacZ-K19^{CreERT}*) or *TC-K19^{CreERT}* mice (*TC-LacZ-K19^{CreERT}*), and recombined cells were labeled with LacZ. At 3.5 wk after TAM administration in *KTC-LacZ-K19^{CreERT}* mice, LacZ was expressed in most cancer cells but in few surface BECs (Fig. 2*D*). Also in *TC-LacZ-K19^{CreERT}* mice, LacZ$^+$ cells were few in the surface BECs but remained in the PBGs (Fig. 2*D*). In contrast, *LacZ-K19^{CreERT}* mice and *KT-K19^{CreERT}* mice crossed with *Rosa26-LSL-LacZ* mice (*KT-LacZ-K19^{CreERT}*), in which E-cadherin was not deleted in BECs, retained many LacZ$^+$ cells in the surface BECs at the same time point (Fig. 2*D*). Based on these findings, we considered that E-cadherin–deleted surface BECs might not survive for long periods and that the remaining recombined cells in the PBGs might give rise to ECC.

Time Course of Histological Progression of ECC. To assess this hypothesis, the time course of histological changes in the EHBD of *KTC-K19^{CreERT}* mice after TAM administration was analyzed. On day 5, although the EHBD was mostly normal, the alignment of the surface BECs was partially disrupted (Fig. 3*A*). On day 7, surface BECs started to detach from the BD wall, and on day 10, many shedding BECs were observed in the BD lumen, and inflammatory cells had infiltrated the subepithelial connective tissue (Fig. 3*A*). The inflammatory reaction was seen throughout the entire EHBD but was slightly dominant in the upper CBD. (Fig. 3*A* and Fig. S5*A*). Notably, the PBGs were enlarged and morphologically dysplastic and accompanied by mitotic figures (Fig. 3 *A* and *B*). On day 15, although the shedding of surface BECs had subsided, the cancerous glands spread through the subepithelial area, accompanied by a fibrotic response (Fig. 3*A*). Wall thickening due to cancerous glands was dominantly seen around the insertion site of the cystic duct, where PBGs are abundant (Fig. S5*B*). Most of the histological features of periductal infiltrating-type ECC were completed by day 20 (Fig. 3*A*). In contrast, TAM-administered Cre-negative *KTC* mice did not show histological changes in the EHBD during this period (Fig. S5*C*).

Next, the time course of E-cadherin expression in BECs was assessed by IHC. E-cadherin was deleted in ∼30% of surface BECs and PBGs on day 5 and efficiently deleted in the area with disrupted epithelial alignment (Fig. 3*C*). On day 10, many E-cadherin–deleted surface BECs were falling into the BD lumen, and as a consequence, the number of E-cadherin–deleted surface BECs was decreased (Fig. 3*C*). In contrast, the PBGs retained many E-cadherin–deleted cells, and some PBGs were replaced completely by E-cadherin–negative cells (Fig. 3*C*). On day 15, most surface BECs had been replaced by E-cadherin–positive cells, whereas E-cadherin–negative cancerous glands had spread in the subepithelial area (Fig. 3*C*). Additionally, recombined cells were monitored by LacZ staining using *KTC-LacZ-K19^{CreERT}* mice. As expected, the timing of the series of events in LacZ$^+$ cells was similar to that in E-cadherin–negative cells (Fig. 3*D*). Furthermore, *C-K19^{CreERT}* mice crossed with *Rosa26-LSL-LacZ* mice (*C-LacZ-K19^{CreERT}*) showed detachment of LacZ$^+$ BECs on day 10, whereas *KT-LacZ-K19^{CreERT}* mice did not, indicating that loss of E-cadherin was responsible for the detachment of BECs (Fig. S5*D*). On the other hand, the perihilar and peripheral IHBD in *KTC-K19^{CreERT}* mice retained E-cadherin–deleted/LacZ$^+$ surface BECs at 3.5 wk after TAM administration (Fig. S5*E*), although the reason for the difference between the EHBD and IHBD was unclear.

Next, cell proliferation was analyzed by Ki67 staining. On day 7, the number of Ki67-positive cells among both the surface BECs and PBGs increased significantly, probably reflecting a regenerative response to the biliary epithelial injury (Fig. 3*E*). Double staining of E-cadherin and Ki67 revealed that cells in the PBGs were highly proliferative irrespective of their E-cadherin expression, whereas the majority of proliferating surface BECs were E-cadherin–positive (Fig. 3*F* and Fig. S5*F*). Furthermore, on day 10, a more marked proliferative response was observed, especially in PBGs, including E-cadherin–deleted PBGs (Fig. 3 *E* and *F*). Hyperproliferative response in *KTC-K19^{CreERT}* mice was confirmed by immunostaining of the mitotic marker phosphohistone 3 (Fig. S5*G*). Additionally, the number of Ki67-positive cells in *KTC-K19^{CreERT}* mice was much higher than that in *KT-K19^{CreERT}* mice at the same time point (Fig. S5*H*), further supporting the contribution of E-cadherin loss-induced biliary epithelial injury to the hyperproliferative response in *KTC-K19^{CreERT}* mice. On day 15, the number of Ki67-positive BECs decreased significantly, whereas E-cadherin–negative cancerous glands were highly proliferative (Fig. 3 *E* and *F*). Thus, E-cadherin–deleted surface BECs detached from the wall of the EHBD, which induced a regenerative response by PBGs. Recombined cells survived among PBGs, which were thus likely the cellular origins of ECC.

Establishment of Biliary Organoid-Derived Cancer Model. To further elucidate the molecular mechanisms of ECC development in *KTC-K19^{CreERT}* mice, we cultured the biliary organoid from the EHBD of Cre-negative *KTC* mice (19) and induced gene recombination using a lentivirus expressing Cre-recombinase (Cre$^+$ *KTC* organoid) or a control lentivirus (Cre$^-$ *KTC* organoid) (Fig. 4*A*). As shown in Fig. 4*B*, lentivirus efficiently induced gene recombination. Then Cre$^+$ *KTC* organoids and Cre$^-$ *KTC* organoids were transplanted subcutaneously into nude mice. Two months later, 66.7% (8/12) of Cre$^+$ *KTC* organoids formed s.c. tumors with a histology similar to that of ECC in *KTC-K19^{CreERT}* mice, whereas none (0/12) of the Cre$^-$ *KTC* organoids formed tumors (Fig. 4*C*), indicating that Cre$^+$ *KTC* organoids possess a tumorigenic ability similar to that of the in vivo model. Furthermore, the tumorigenic abilities of the biliary organoids derived from *K*, *T*, *C*, *KT*, *KC*, and *TC* mice, in which recombination was induced by lentivirus infection, were evaluated in the same way. As shown in Fig. 4*D*, none of the organoids, with the exception of 2/12 (16.7%) *TC* organoids, produced s.c. tumors, suggesting that mutations in Kras, TGFβR2, and E-cadherin cooperatively promote tumorigenesis also in the organoid-derived cancer model.

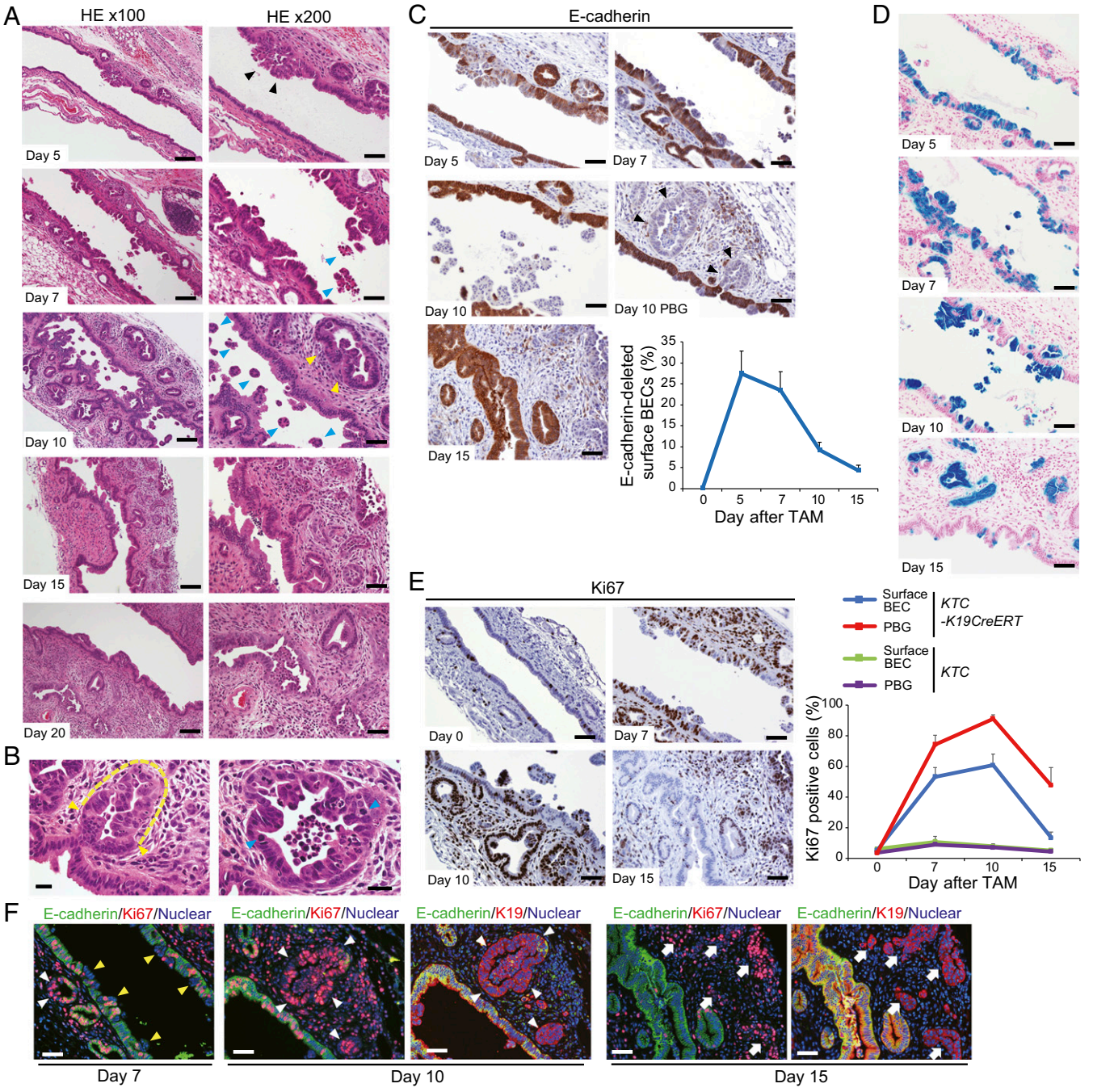

Fig. 3. Histological progression of ECC. (*A*) H&E-stained images of the EHBD (middle to upper area of CBD) of *KTC-K19*^{CreERT} mice after TAM administration at the indicated time points. (Scale bar: *Left* panels, 100 μm; *Right* panels, 50 μm.) Black arrowheads, disrupted epithelial alignment; blue arrowheads, BECs detaching from the bile duct epithelium; yellow arrowheads, enlarged and dysplastic PBGs. (*B*) High-magnification images of PBGs in *KTC-K19*^{CreERT} mice on day 10. (Scale bar: 20 μm.) Yellow dashed line represents dysplastic cells in the PBGs, and yellow arrowheads indicate the border between the dysplastic PBG cells and normal surface BECs. Blue arrowheads indicate mitotic cells. (*C*) Time course of E-cadherin expression in the EHBD of *KTC-K19*^{CreERT} mice after TAM administration. (Scale bar: 50 μm.) Black arrowheads indicate E-cadherin–negative PBGs. Line graph shows percentage of E-cadherin–deleted BECs on the luminal surface of the EHBD of *KTC-K19*^{CreERT} mice after TAM administration (means ± SD, $n = 3$ per time point). (*D*) LacZ-stained images of the EHBD of *KTC-LacZ-K19*^{CreERT} mice at various time points after TAM administration. (Scale bar: 50 μm.) (*E*) Ki67 expression in the EHBD of *KTC-K19*^{CreERT} mice at various time points after TAM administration. (Scale bar: 50 μm.) Line graph shows percentage of Ki67-positive cells in the EHBD of *KTC* and *KTC-K19*^{CreERT} mice after TAM administration (means ± SD, $n = 3$ per time point). Surface BECs and PBGs were analyzed separately. (*F*) Double IF-stained images of E-cadherin and Ki67 in the EHBD of *KTC-K19*^{CreERT} mice after TAM administration. (Scale bar: 50 μm.) To locate the E-cadherin–deleted duct cells, double IF-stained images of E-cadherin and K19 in serial sections from mice killed on days 10 and 15 are shown. Yellow arrowheads, E-cadherin–deleted nonproliferating surface BECs; white arrowheads, E-cadherin–deleted proliferating cells in PBGs; white arrows, E-cadherin–deleted proliferating cancerous glands.

Cre^{+} *KTC* organoids also formed s.c. tumors in syngeneic C57BL/6 mice (5/8, 62.5%) (Fig. S6*A*). Of particular interest, as was the case in vivo, hematoxylin and eosin (H&E) staining of organoids revealed loss of E-cadherin–induced BECs shedding, which was most evident in *KTC* organoids (Fig. 4*E*). Thus, this system recreates the in vivo conditions and facilitates analysis of carcinogenesis

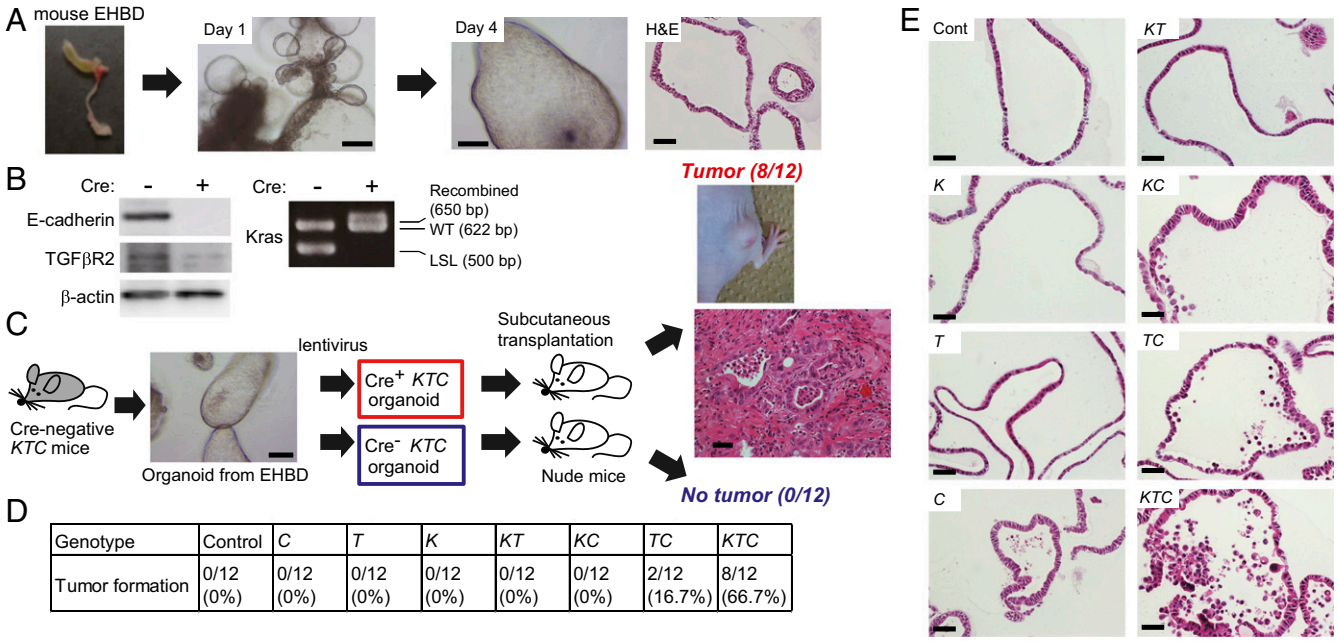

Genotype	Control	C	T	K	KT	KC	TC	KTC
Tumor formation	0/12 (0%)	0/12 (0%)	0/12 (0%)	0/12 (0%)	0/12 (0%)	0/12 (0%)	2/12 (16.7%)	8/12 (66.7%)

Fig. 4. Establishment of biliary organoid-derived cancer. (*A*) Micrograph and H&E-stained image of biliary organoids cultured from the EHBD of mice. (Scale bar: micrographs, 250 μm; H&E staining, 50 μm.) (*B*) Confirmation of recombination by Cre-expressing lentivirus in organoids from *KTC* mice. The indicated proteins were assessed by Western blot. Cre-mediated recombination of the *LSL-Kras* allele was confirmed by PCR. (*C*) Biliary organoids from the EHBD of *KTC* mice were infected with Cre-expressing or control lentivirus and then transplanted subcutaneously into nude mice. An H&E-stained image of an organoid-derived tumor is shown. (Scale bar: 50 μm.) (*D*) EHBD organoids from the indicated mice were infected with lentivirus and then transplanted subcutaneously into nude mice. Tumor formation was assessed 2 mo after transplantation. (*E*) H&E-stained images of EHBD organoids from the indicated mice after gene recombination. (Scale bar: 50 μm.)

induced by genetic manipulations in BECs separately from the tumor microenvironment.

IL-33 Links Biliary Epithelial Injury, Regeneration, and Cholangiocarcinogenesis in *KTC-K19^{CreERT}* Mice. Next, a cDNA microarray analysis was conducted using Cre$^+$ *KTC* and Cre$^-$ *KTC* organoids. A total of 1,096 genes were up- or down-regulated at least twofold in Cre$^+$ *KTC* organoids compared with Cre$^-$ *KTC* organoids (Fig. 5*A*). Among these genes, we focused on IL-33, which exhibited the 13th highest magnitude of up-regulation. IL-33 is a member of the IL-1 family originally described as an inducer of type 2 innate immunity (20), and it was recently reported to promote BEC proliferation particularly in the EHBD (21). Real-time PCR revealed an ∼75-fold increase in IL-33 mRNA levels in Cre$^+$ *KTC* organoids compared with Cre$^-$ *KTC* organoids. IL-33 expression was mildly increased by Kras activation (∼2-fold), moderately increased by deletion of TGFβR2 or E-cadherin (∼10-fold), and markedly increased by all three manipulations combined (Fig. 5*B*), suggesting that three genes cooperatively up-regulated IL-33.

Consistent with a previous report (21), i.p. administration of IL-33 (1 μg) for 3 d to C57BL/6 wild-type (WT) mice induced hyperplasia of surface BECs and expansion of PBGs in the EHBD on day 5 but had little effect on the peripheral IHBD or GB (Fig. S6*B*). Ki67 staining revealed marked proliferation of BECs in the EHBD, especially in PBGs (Fig. S6*C*).

KTC-K19^{CreERT} mice revealed increased IL-33 mRNA levels in ECC tissues and increased IL-33 protein levels in the bile and serum compared with control *KTC* mice (Fig. 5*C*). Immunofluorescence (IF) analysis of *KTC-K19^{CreERT}* mice on day 5 after TAM administration revealed increased expression of IL-33 in the nucleus of E-cadherin–deleted BECs, especially those in the area of disrupted alignment (Fig. 5*D*), and on day 10, some E-cadherin–negative detached BECs also strongly expressed nuclear IL-33 (Fig. S6*D*). Of note, IL-33 also functions as an "alarmin," released from dying cells as an indicator of infection or tissue injury (20). Actually, although cell lines established from Cre$^+$ *KTC* biliary organoids (termed "KTC-BO cells") did not secrete IL-33, necrosis due to repeated freeze–thaw cycles led to release of IL-33 (Fig. S6*E*). Therefore, release of excess IL-33 from dying BECs may play a key role in regeneration of the EHBD and subsequent carcinogenesis in *KTC-K19^{CreERT}* mice. Additionally, cancer glands in *KTC-K19^{CreERT}* mice exhibited abundant luminal necrosis, and necrotic cells expressed IL-33 (Fig. S6*F*), suggesting that luminal necrosis might contribute to persistent IL-33 release even after ECC development in *KTC-K19^{CreERT}* mice. Furthermore, we examined the expression of IL-33 in human ECC samples analyzed in Fig. 1*E*; 71.4% (5/7) of samples with an expression pattern similar to the mouse model (phospho-ERK–positive, SMAD4-negative, and E-cadherin–negative) expressed IL-33, whereas 24.2% (7/29) of the remaining patients were IL-33–positive ($P = 0.028$) (Fig. S6*G*). Additionally, cancer cells undergoing luminal necrosis expressed IL-33 (Fig. S6*H*). These findings are consistent with those in mice. We also performed terminal deoxynucleotidyl transferase-mediated dUTP nick end labeling (TUNEL) staining in EHBD tissue from *KTC-K19^{CreERT}* mice on day 10 after TAM administration. Many TUNEL-positive cells were found in the subepithelial areas and were identified as K19$^-$/CD45$^+$ immune cells (Fig. S6*I*). However, most of the detached BECs were TUNEL-negative, suggesting that the detached BECs were undergoing a form of cell death other than apoptosis. In fact, it has been shown that IL-33 is released during necrosis and cellular stress, but during apoptosis, caspase-mediated cleavage of IL-33 diminishes the biological activity of IL-33 (22).

A previous study reported that IL-33–induced proliferation of BECs was mediated by type 2 innate lymphoid cells (ILC2s) (21). Thus, the number of hepatic ILC2s in *KTC-K19^{CreERT}* mice was determined by flow cytometry. As expected, the number of ILC2s, defined as lineage$^-$ (CD3$^-$, Gr1$^-$, CD11b$^-$, CD45R$^-$, Ter119$^-$),

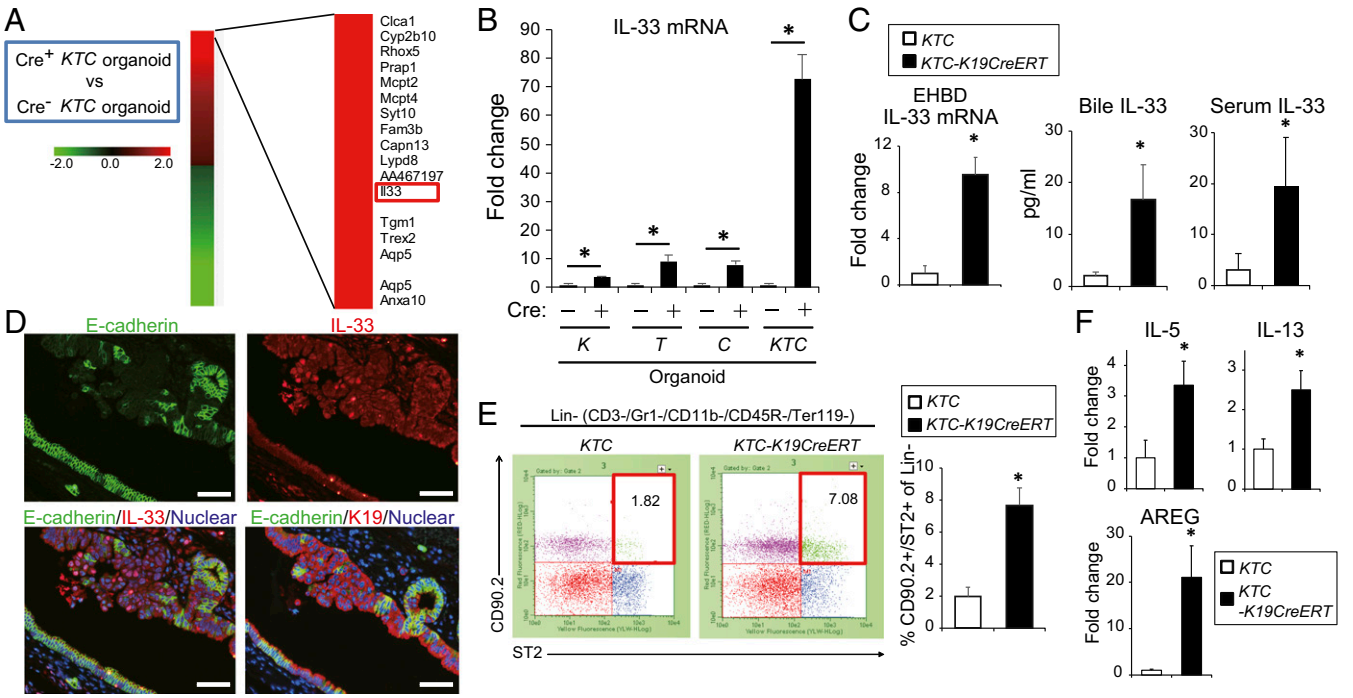

Fig. 5. IL-33 links biliary epithelial injury, regeneration, and cholangiocarcinogenesis. (*A*) cDNA microarray analysis of Cre$^+$ *KTC* and Cre$^-$ *KTC* organoids. A total of 1,096 genes were at least twofold up- or down-regulated in Cre$^+$ *KTC* organoids. The top 20 up-regulated genes are shown. (*B*) EHBD organoids from the indicated mice were infected with control or Cre-expressing lentivirus, and relative IL-33 mRNA levels were determined by real-time PCR. Bar graph shows the relative IL-33 mRNA levels after infection with Cre-expressing lentivirus compared with the control lentivirus (means ± SD, $n = 3$ per group). *$P < 0.05$. (*C*) Relative IL-33 mRNA levels in EHBDs obtained from *KTC* and *KTC-K19^{CreERT}* mice at 3.5 wk after TAM administration were determined by real-time PCR ($n = 3$ per group), and IL-33 protein levels in the bile and serum of *KTC* and *KTC-K19^{CreERT}* mice at 3.5 wk after TAM administration were measured by ELISA (bile, $n = 5$ per group; serum, $n = 8$ per group). Data are means ± SD. *$P < 0.05$. (*D*) Double IF staining of E-cadherin and IL-33 in the EHBD of *KTC-K19^{CreERT}* mice on day 5. (Scale bar: 50 μm.) To locate E-cadherin–deleted duct cells, double IF staining of E-cadherin and K19 in serial sections is also shown. (*E*) Numbers of hepatic ILC2s in *KTC* and *KTC-K19^{CreERT}* mice on day 20 after TAM administration were analyzed by flow cytometry. Representative dot plots and numbers from three independent experiments (bar graph) are shown (means ± SD; $n = 3$ per group). *$P < 0.05$. (*F*) Relative IL-5, IL-13, and AREG mRNA levels were determined by real-time PCR in EHBDs from *KTC* and *KTC-K19^{CreERT}* mice at 3.5 wk after TAM administration (means ± SD; $n = 3$ per group). *$P < 0.05$.

ST2$^+$, and CD90.2$^+$ cells, was significantly increased in *KTC-K19^{CreERT}* mice compared with *KTC* mice (Fig. 5*E*). IF analysis confirmed the accumulation of CD45$^+$, ST2$^+$ cells in the subepithelial tissue of the EHBD of TAM-administered *KTC-K19^{CreERT}* mice (Fig. S6*J*). In addition, infiltration of CD45$^+$, ST2$^+$ cells was seen in xenografts derived from Cre$^+$ *KTC* organoids, and we confirmed that the IL-33–induced proliferative response of BECs was conserved in nude mice (Fig. S6 *K* and *L*).

ILC2s have been reported to produce the effector cytokines IL-4, IL-5, IL-9, IL-13, and amphiregulin (AREG) in response to IL-33 (20), among which IL-13 was reported to contribute to proliferation of BECs (21). Although IL-4 and IL-9 mRNAs were not detected by real-time PCR, the expression levels of IL-5, IL-13, and AREG mRNA were significantly increased in the ECC tissues of *KTC-K19^{CreERT}* mice compared with control EHBD tissues of *KTC* mice (Fig. 5*F*). In particular, AREG expression was markedly increased in *KTC-K19^{CreERT}* mice. Administration of IL-33 to WT mice also significantly increased the expression of AREG in the EHBD (Fig. S7*A*). AREG is a ligand for epidermal growth factor receptor and has been reported to be involved in the repair of intestinal and lung tissues as an effector of the IL-33–ILC2 axis (23, 24). In fact, i.p. administration of AREG (10 μg for 3 consecutive days) to WT mice significantly increased the number of Ki67-positive cells among surface BECs and in the PBGs (Fig. S7*B*). Additionally, AREG promoted proliferation of KTC-BO cells and the human ECC TFK1 cells in vitro (Fig. S7*C*). These findings suggest that AREG contributes to proliferation of BECs as effectors of the IL-33 pathway.

IL-33 Can Substitute for Loss of E-Cadherin in the Development of ECC and Be a Therapeutic Target. If IL-33 released from dying BECs as a result of E-cadherin loss plays a critical role in ECC development, administration of IL-33 may be able to substitute for loss of E-cadherin. To test this hypothesis, IL-33 was administered to TAM-administered *KT-K19^{CreERT}* mice or Cre-negative *KT* mice on days 10, 11, and 12, and the histology of the liver and BD was analyzed on day 28 (Fig. S8*A*). Surprisingly, IL-33–administered *KT-K19^{CreERT}* (*KT-K19^{CreERT}*+IL-33) mice exhibited a markedly thickened EHBD, whereas IL-33–administered Cre-negative *KT* mice showed only mild expansion of PBGs at this time point (Fig. 6*A*). *KT-K19^{CreERT}*+IL-33 mice revealed not only proliferation of dysplastic glands in the subepithelial tissue of the EHBD but also papillary tumors arising from surface BECs, probably because E-cadherin was not deleted in the BECs of *KT-K19^{CreERT}* mice (Fig. 6*A*). In fact, in contrast to *KTC-LacZ-K19^{CreERT}* mice, both dysplastic PBGs and papillary tumors occurring in IL-33–administered *KT-LacZ-K19^{CreERT}* mice expressed LacZ (Fig. 6*B*). Additionally, we confirmed that the number of hepatic ILC2s in *KT-K19^{CreERT}*+IL-33 mice was increased significantly compared with control *KT-K19^{CreERT}* mice even 1 wk after initial IL-33 administration (Fig. S8). Thus, IL-33 cooperates with Kras and TGFβR2 mutations in the development of biliary tumors. Notably, neoplastic changes in BECs extended to the intrahepatic hilar area but not to the peripheral IHBD in *KT-K19^{CreERT}*+IL-33 mice (Fig. 6*C*). Such a distribution was consistent with that in *KTC-K19^{CreERT}* mice. Therefore, differences in the reactivity to IL-33 among the components of the biliary tree may explain the distribution of CC in *KTC-K19^{CreERT}* mice.

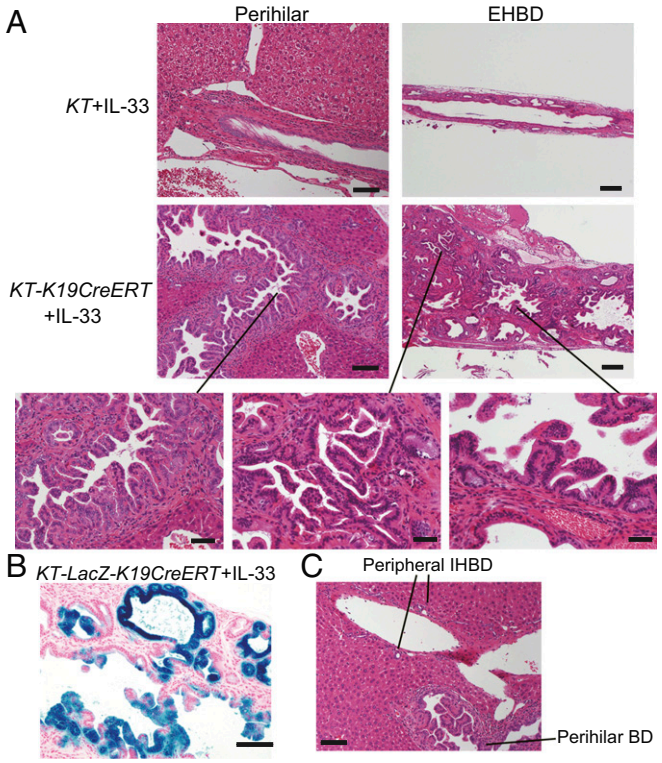

Fig. 6. IL-33 cooperates with Kras and TGFβR2 mutations in the development of biliary tumors. (*A*) H&E-stained images of EHBDs and perihilar BDs from IL-33–administered *KT* and *KT-K19*^{CreERT} mice. (Scale bar: *Left* panels, 100 μm; *Right* panels, 200 μm; *Lower* panels, 50 μm.) (*B*) LacZ-stained image of the EHBD of *KT-LacZ-K19*^{CreERT} mice administered IL-33 using the protocol described in Fig. S8*A*. (Scale bar: 100 μm.) (*C*) H&E staining of the liver, including the perihilar and peripheral BD, of *KT-K19*^{CreERT}+IL-33 mice. (Scale bar: 100 μm.)

Next, we treated *KTC-K19*^{CreERT} mice with a neutralizing anti–IL-33 antibody (Fig. 7*A*) (25). Anti–IL-33 treatment significantly attenuated the thickening of the EHBD wall (Fig. 7 *B* and *C*) and decreased the frequency of mice with a serum total bilirubin level greater than 2 mg/mL (30% vs. 0%) and IHBD dilatation (Fig. 7*D*). AREG and IL-13 mRNA levels and the number of hepatic ILC2s were also decreased by anti–IL-33 treatment (Fig. 7 *E* and *F*). Additionally, anti–IL-33 treatment significantly suppressed the hyperproliferative response of BECs on day 10 (Fig. 7*G*). These results indicate that the excess IL-33–mediated hyperproliferative response to biliary epithelial injury contributes to ECC development in *KTC-K19*^{CreERT} mice (Fig. 7*H*). Furthermore, anti–IL-33 treatment suppressed the growth of KTC-BO tumors xenografted into C57BL/6 mice (Fig. S9 *A–C*). Thus, IL-33 may be a potential therapeutic target for ECC.

Loss of E-Cadherin–Mediated Yes-Associated Protein Activation Promotes ECC Proliferation and Invasion. Although the above findings demonstrate that IL-33 can promote cholangiocarcinogenesis and substitute for loss of E-cadherin in the development of ECC, tumors in *KT-K19*^{CreERT}+IL-33 mice were less aggressive than were those in *KTC-K19*^{CreERT} mice and did not show lymphatic invasion or metastasis. Thus, whether loss of E-cadherin contributes to cholangiocarcinogenesis through not only biliary epithelial injury but also activation of the intrinsic oncogenic pathway was evaluated next. Loss of E-cadherin has been reported to induce nuclear translocation of β-catenin (26), which promotes carcinogenesis. However, expression of nuclear β-catenin was not increased despite decreased membranous β-catenin in the ECC cells of *KTC-K19*^{CreERT} mice (Fig. S10*A*). In contrast, Yes-associated protein (YAP) expression, which plays an important role in cholangiocarcinogenesis (27) and is reportedly activated by loss of E-cadherin (28), was significantly increased in ECC cells (Fig. S10*B*). Microarray analysis of the biliary organoids performed in Fig. 5 also showed increased expression of YAP downstream oncogenes in Cre^{+} *KTC* organoids, such as Birc5 (4.75-fold), Foxm1 (4.38-fold), and Cyclin D1 (2.08-fold). In fact, knockdown of E-cadherin in TFK1 cells inactivated the Hippo-signaling cascade, which induces YAP degradation, resulting in increased nuclear accumulation of YAP (Fig. S10*C*). Knockdown of E-cadherin in TFK1 cells promoted their proliferation and accumulation without contact inhibition, but those effects were attenuated by knockdown of YAP (Fig. S10 *D–F*). Furthermore, the invasion capacity was significantly increased by knockdown of E-cadherin in TFK1 cells, which was inhibited by additional knockdown of YAP (Fig. S10*G*). Knockdown of YAP in KTC-BO cells also significantly attenuated their proliferation and down-regulated the expression of Birc5 and Foxm1 (Fig. S10 *H–J*). The YAP inhibitor verteporfin significantly suppressed ECC development in *KTC-K19*^{CreERT} mice in vivo (Fig. S10*K*). Thus, loss of E-cadherin–mediated YAP activation is also implicated in ECC development.

Discussion

In the present study, a mouse model of biliary injury-related ECC was established through duct-cell–specific activation of Kras and deletion of TGFβR2 and E-cadherin. To our knowledge, two genetically engineered mouse models have been reported to develop extrahepatic biliary tumors: ErbB-2 transgenic mice and duct-cell–specific Kras-activation and PTEN-deletion mice (11, 29). Although these mice were reported as models of GB cancer and ICC, respectively, they also developed well-differentiated papillary tumors in the EHBD. In contrast, ECC in *KTC-K19*^{CreERT} mice spread laterally along the biliary tree, and cancer cells were highly malignant and metastasized to the regional lymph nodes. Periductal infiltrating growth and lymph node metastasis are characteristics of human ECC and responsible for its poor prognosis. Therefore, our mouse model is clinically relevant and will facilitate investigation of the pathogenesis of human ECC.

Death-driven compensatory proliferation to repair tissue defects is an important promoter of inflammation-associated carcinogenesis (30), and the mechanism underlying this process has been well analyzed in hepatocellular carcinoma (31, 32). However, although CC also occurs in the presence of chronic biliary injury and inflammation (2), the mechanism is unclear. In *KTC-K19*^{CreERT} mice, the surface BECs detached from the wall of the EHBD due to loss of E-cadherin, which subsequently induced inflammation and a regenerative response by the remaining BECs, especially in PBGs. However, cells harboring mutations survived in the PBGs; therefore, the regenerative response to biliary injury resulted in ECC development from PBGs. Importantly, significant proliferation and hyperplasia of PBGs in response to biliary injury were observed in patients with primary sclerosing cholangitis and liver fluke infection (33, 34). Furthermore, the PBGs of patients with hepatolithiasis frequently harbor Kras mutations (35). Thus, a chronic biliary epithelial injury-induced proliferative response may result in development of CC from PBGs in humans, and this study provides experimental evidence of this possibility.

We succeeded in culturing biliary organoids following gene recombination capable of forming s.c. tumors, in which we identified IL-33 as a key factor linking biliary epithelial injury, regeneration, and cholangiocarcinogenesis. IL-33 was up-regulated in BECs cooperatively by mutations of Kras, TGFβR2, and E-cadherin. Although the mechanisms of regulation of IL-33 expression remain unclear, Kras activation and TGFβR2 inactivation have been reported to up-regulate IL-33 expression in the lung and

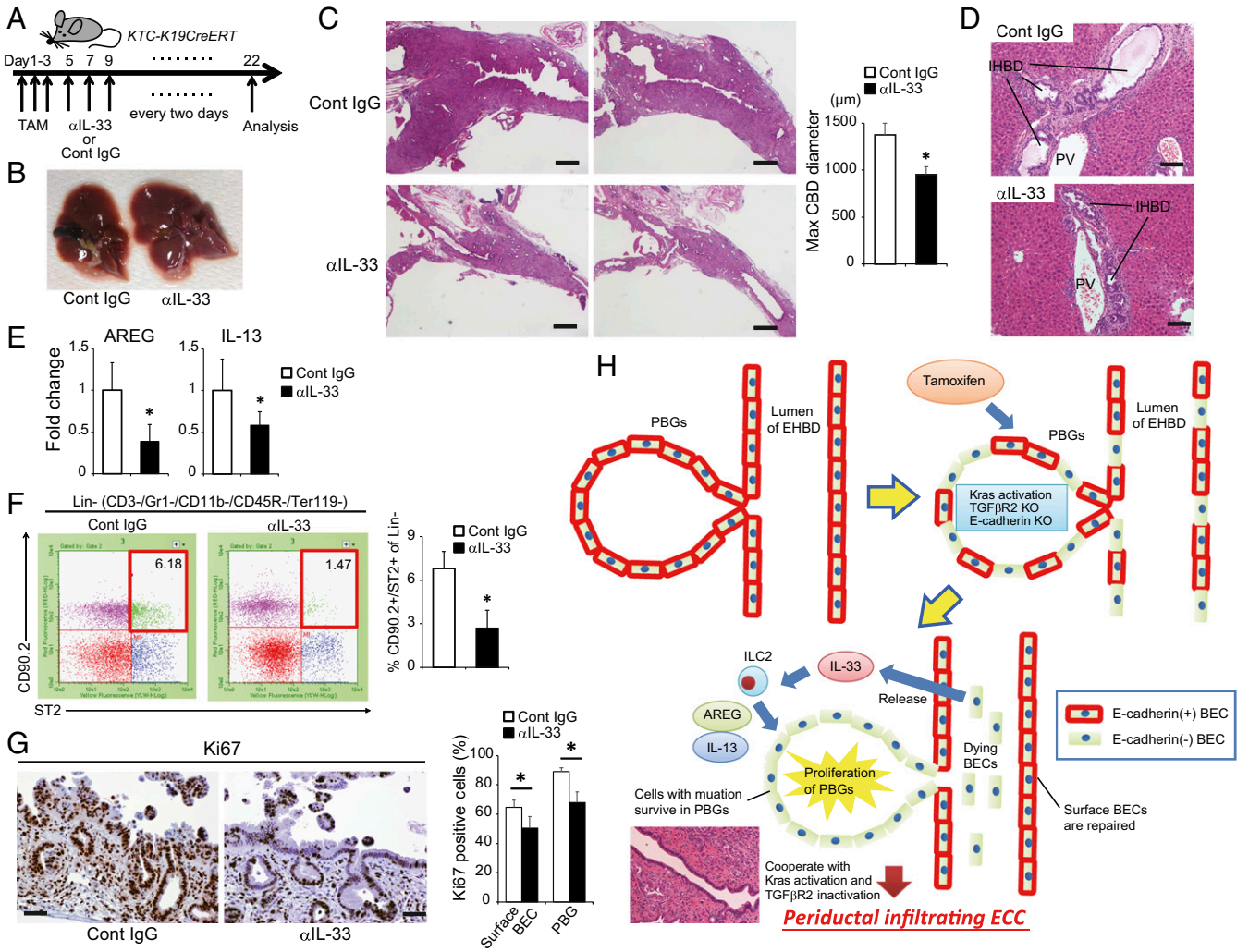

Fig. 7. Blocking IL-33 suppresses ECC development. (*A*) Protocol of anti–IL-33 treatment of *KTC-K19^{CreERT}* mice. (*B* and *C*) Representative macroscopic (*B*) and H&E-stained (*C*) images of EHBDs from *KTC-K19^{CreERT}* mice treated with anti–IL-33 antibody or control IgG. (Scale bar: 500 μm.) Bar graph shows maximum diameter of the CBD (means ± SEM; $n = 10$ per group). *$P < 0.05$. (*D*) H&E-stained images of the IHBDs of anti–IL-33- or control IgG-administered *KTC-K19^{CreERT}* mice. (Scale bar: 100 μm.) (*E*) Relative AREG and IL-13 mRNA levels in EHBDs from anti–IL-33 or control IgG-administered *KTC-K19^{CreERT}* mice were determined by real-time PCR (means ± SD; $n = 6$ per group). *$P < 0.05$. (*F*) Numbers of hepatic ILC2s in anti–IL-33- or control IgG-administered *KTC-K19^{CreERT}* mice on day 20 after TAM administration were analyzed by flow cytometry. Representative dot plots and numbers from three independent experiments (bar graph) are shown (means ± SD; $n = 3$ per group). *$P < 0.05$. (*G*) Representative Ki67-stained image of anti–IL-33 or control IgG-administered *KTC-K19^{CreERT}* mice on day 10 after TAM administration. (Scale bar: 50 μm.) Bar graph shows the frequencies of Ki67-positive cells among the surface BECs and in PBGs (means ± SD; $n = 5$ per group). *$P < 0.05$. (*H*) Proposed mechanism of ECC development in *KTC-K19^{CreERT}* mice.

macrophages, respectively (36, 37). In addition, disruption of the integrity of the lung and skin epithelial barrier has been reported to induce production of IL-33 (38). IL-33 functions as a sensor of epithelial barrier injury due to invasion of pathogens, including helminths, and induces a Th2 immune response to eliminate pathogens and repair the injured tissue through ILC2 activation (20). In this sense, loss of cell–cell adhesion due to E-cadherin deletion in BECs could trigger up-regulation of IL-33. Interestingly, a recent study showed significantly increased biliary epithelial IL-33 expression and serum IL-33 levels in patients with liver helminth *Clonorchis sinensis* infection (39). Together with our data, IL-33 may be a link between helminth infection and CC development. The finding that blocking IL-33 significantly suppressed ECC development in our study suggests IL-33 as a potential therapeutic target for ECC. Additionally, AREG, a downstream target of IL-33, should also be explored as another candidate for a therapeutic target for ECC in the future.

We showed that only three administrations of IL-33 to *KT-K19^{CreERT}* mice was sufficient to induce biliary tumors. Although it is unknown why transient administration of IL-33 was sufficient for tumor development, a recent study showed that intranasal injection of IL-33 induced a sustained increase in lung ILC2s for more than 4 wk, albeit at a low level, and once ILC2s were primed by IL-33, they were highly responsive, even to unrelated allergens, and strongly induced inflammation (40). Thus, ILC2s primed by IL-33 may exert a long-term effect on the BD of *KT-K19^{CreERT}* mice.

The distribution of CC is a unique characteristic of this mouse model. CC in *KTC-K19^{CreERT}* mice was seen predominantly in the EHBD and perihilar IHBD, despite similar recombination efficiency among the biliary tree. This difference may be due, at least in part, to IL-33, for the following reasons. First, exogenous administration of IL-33 induced inflammation and BEC proliferation in the EHBD and perihilar BD, whereas the peripheral IHBD and GB were largely unaffected. This finding suggests that

reactivity to IL-33 differs among regions of the biliary tree. Second, IL-33 is released from dying cells, and the shedding of BECs was more prominent in the EHBD than in the IHBD in *KTC-K19*^{CreERT} mice. Thus, the level of IL-33 released from dying cells might be greater in the EHBD than in the IHBD. However, the peripheral IHBD and EHBD/large IHBD are embryologically different and thus may exhibit distinct properties other than IL-33 signaling.

PBGs have attracted attention as a BEC stem-cell niche and a potential origin of ECC (10). In the present study, IHC analysis of E-cadherin and lineage-tracing of LacZ-labeled cells suggests that ECC can originate from cells in the PBGs. Indeed, the distribution of CC in *KTC-K19*^{CreERT} mice largely corresponded with that of PBGs (i.e., EHBD and perihilar BD). However, to definitively determine this issue, experiments using PBG-specific gene recombination are needed. Because a specific marker of PBGs has not been identified in mice, this remains a subject of future investigations.

Several studies have suggested that floxed alleles exhibit differential sensitivities to Cre-mediated recombination (41), but we were unable to perform histological assessment of *LSL-Kras*^{G12D} and *Tgfbr2*$^{flox/flox}$ allele recombination because of a lack of antibodies appropriate for immunostaining. This raises the question of whether specific combinations of recombination have a greater propensity to induce malignancy. The findings that only *KTC-K19*^{CreERT} mice developed ECC and most of the organoids other than *KTC* organoids could not form s.c. tumors suggest that all of the alleles would be recombined in cancer cells. However, further analysis is needed to obtain conclusive evidence.

In conclusion, we established a mouse model of biliary injury-related ECC. This model provided insight into the carcinogenic mechanisms, cellular origin, and potential therapeutic targets of ECC.

Materials and Methods

Albumin-Cre, *LSL-Kras*^{G12D}, *CDH1*$^{flox/flox}$, and *Rosa26-LSL-tdTomato* mice were purchased from the Jackson Laboratory. *K19*^{CreERT}, *Tgfbr2*$^{flox/flox}$, and *Rosa26-LSL-LacZ* mice have been described previously (13, 14, 42). All mice were of the C57BL/6 genetic background. Nude mice were purchased form CLEA Japan. All experiments were approved by the Ethics Committee for Animal Experimentation of the University of Tokyo and the Institute for Adult Diseases, Asahi Life Foundation, and were conducted in accordance with the *Guide for the Care and Use of Laboratory Animals* (43). Human ECC samples were obtained from 36 patients who underwent surgical treatment at The University of Tokyo Hospital with informed consent. This study was approved by the Ethics Committee of the University of Tokyo. Other methods are described in *SI Materials and Methods*.

ACKNOWLEDGMENTS. This study was supported by the Japanese Society for the Promotion of Science Kakenhi Grant 15K09039; the Astellas Foundation for Research on Metabolic Disorders; the Nakayama Cancer Research Institute; the Okinaka Memorial Institute for Medical Research; a research grant from the Princess Takamatsu Cancer Research Fund; and the Foundation for Promotion of Cancer Research in Japan.

1. Rizvi S, Gores GJ (2013) Pathogenesis, diagnosis, and management of cholangiocarcinoma. *Gastroenterology* 145:1215–1229.
2. Malhi H, Gores GJ (2006) Cholangiocarcinoma: Modern advances in understanding a deadly old disease. *J Hepatol* 45:856–867.
3. Chan-On W, et al. (2013) Exome sequencing identifies distinct mutational patterns in liver fluke-related and non-infection-related bile duct cancers. *Nat Genet* 45: 1474–1478.
4. Nakamura H, et al. (2015) Genomic spectra of biliary tract cancer. *Nat Genet* 47: 1003–1010.
5. Roskams T, Desmet V (2008) Embryology of extra- and intrahepatic bile ducts, the ductal plate. *Anat Rec (Hoboken)* 291:628–635.
6. Sekiya S, Suzuki A (2012) Intrahepatic cholangiocarcinoma can arise from Notch-mediated conversion of hepatocytes. *J Clin Invest* 122:3914–3918.
7. Fan B, et al. (2012) Cholangiocarcinomas can originate from hepatocytes in mice. *J Clin Invest* 122:2911–2915.
8. Guest RV, et al. (2014) Cell lineage tracing reveals a biliary origin of intrahepatic cholangiocarcinoma. *Cancer Res* 74:1005–1010.
9. Dipaola F, et al. (2013) Identification of intramural epithelial networks linked to peribiliary glands that express progenitor cell markers and proliferate after injury in mice. *Hepatology* 58:1486–1496.
10. Lanzoni G, Cardinale V, Carpino G (2016) The hepatic, biliary, and pancreatic network of stem/progenitor cell niches in humans: A new reference frame for disease and regeneration. *Hepatology* 64:277–286.
11. Ikenoue T, et al. (2016) A novel mouse model of intrahepatic cholangiocarcinoma induced by liver-specific Kras activation and Pten deletion. *Sci Rep* 6:23899.
12. Xu X, et al. (2006) Induction of intrahepatic cholangiocellular carcinoma by liver-specific disruption of Smad4 and Pten in mice. *J Clin Invest* 116:1843–1852.
13. Means AL, Xu Y, Zhao A, Ray KC, Gu G (2008) A CK19(CreERT) knockin mouse line allows for conditional DNA recombination in epithelial cells in multiple endodermal organs. *Genesis* 46:318–323.
14. Ijichi H, et al. (2006) Aggressive pancreatic ductal adenocarcinoma in mice caused by pancreas-specific blockade of transforming growth factor-beta signaling in cooperation with active Kras expression. *Genes Dev* 20:3147–3160.
15. Berx G, van Roy F (2009) Involvement of members of the cadherin superfamily in cancer. *Cold Spring Harb Perspect Biol* 1:a003129.
16. Nitta T, et al. (2014) Prognostic significance of epithelial-mesenchymal transition-related markers in extrahepatic cholangiocarcinoma: Comprehensive immunohistochemical study using a tissue microarray. *Br J Cancer* 111:1363–1372.
17. Nakagawa H, et al. (2014) Loss of liver E-cadherin induces sclerosing cholangitis and promotes carcinogenesis. *Proc Natl Acad Sci USA* 111:1090–1095.
18. Woolbright BL, Jaeschke H (2012) Novel insight into mechanisms of cholestatic liver injury. *World J Gastroenterol* 18:4985–4993.
19. Huch M, et al. (2013) In vitro expansion of single Lgr5+ liver stem cells induced by Wnt-driven regeneration. *Nature* 494:247–250.
20. Molofsky AB, Savage AK, Locksley RM (2015) Interleukin-33 in tissue homeostasis, injury, and inflammation. *Immunity* 42:1005–1019.
21. Li J, et al. (2014) Biliary repair and carcinogenesis are mediated by IL-33-dependent cholangiocyte proliferation. *J Clin Invest* 124:3241–3251.
22. Lüthi AU, et al. (2009) Suppression of interleukin-33 bioactivity through proteolysis by apoptotic caspases. *Immunity* 31:84–98.
23. Monticelli LA, et al. (2015) IL-33 promotes an innate immune pathway of intestinal tissue protection dependent on amphiregulin-EGFR interactions. *Proc Natl Acad Sci USA* 112:10762–10767.
24. Monticelli LA, et al. (2011) Innate lymphoid cells promote lung-tissue homeostasis after infection with influenza virus. *Nat Immunol* 12:1045–1054.
25. Li P, Lin W, Zheng X (2014) IL-33 neutralization suppresses lupus disease in lupus-prone mice. *Inflammation* 37:824–832.
26. Orsulic S, Huber O, Aberle H, Arnold S, Kemler R (1999) E-cadherin binding prevents beta-catenin nuclear localization and beta-catenin/LEF-1-mediated transactivation. *J Cell Sci* 112:1237–1245.
27. Pei T, et al. (2015) YAP is a critical oncogene in human cholangiocarcinoma. *Oncotarget* 6:17206–17220.
28. Kim NG, Koh E, Chen X, Gumbiner BM (2011) E-cadherin mediates contact inhibition of proliferation through Hippo signaling-pathway components. *Proc Natl Acad Sci USA* 108:11930–11935.
29. Kiguchi K, et al. (2001) Constitutive expression of ErbB-2 in gallbladder epithelium results in development of adenocarcinoma. *Cancer Res* 61:6971–6976.
30. Grivennikov SI, Greten FR, Karin M (2010) Immunity, inflammation, and cancer. *Cell* 140:883–899.
31. Maeda S, Kamata H, Luo JL, Leffert H, Karin M (2005) IKKbeta couples hepatocyte death to cytokine-driven compensatory proliferation that promotes chemical hepatocarcinogenesis. *Cell* 121:977–990.
32. Nakagawa H, et al. (2014) ER stress cooperates with hypernutrition to trigger TNF-dependent spontaneous HCC development. *Cancer Cell* 26:331–343.
33. Carpino G, et al. (2015) Activation of biliary tree stem cells within peribiliary glands in primary sclerosing cholangitis. *J Hepatol* 63:1220–1228.
34. Hughes NR, Pairojkul C, Royce SG, Clouston A, Bhathal PS (2006) Liver fluke-associated and sporadic cholangiocarcinoma: An immunohistochemical study of bile duct, peribiliary gland and tumour cell phenotypes. *J Clin Pathol* 59:1073–1078.
35. Hsu M, Sasaki M, Igarashi S, Sato Y, Nakanuma Y (2013) KRAS and GNAS mutations and p53 overexpression in biliary intraepithelial neoplasia and intrahepatic cholangiocarcinomas. *Cancer* 119:1669–1674.
36. Lee S, et al. (2009) Profiling of transcripts and proteins modulated by K-ras oncogene in the lung tissues of K-ras transgenic mice by omics approaches. *Int J Oncol* 34:161–172.
37. Rani R, Smulian AG, Greaves DR, Hogan SP, Herbert DR (2011) TGF-β limits IL-33 production and promotes the resolution of colitis through regulation of macrophage function. *Eur J Immunol* 41:2000–2009.
38. Islam SA, Luster AD (2012) T cell homing to epithelial barriers in allergic disease. *Nat Med* 18:705–715.
39. Yu Q, et al. (2016) Expression and potential roles of IL-33/ST2 in the immune regulation during Clonorchis sinensis infection. *Parasitol Res* 115:2299–2305.
40. Martinez-Gonzalez I, et al. (2016) Allergen-experienced group 2 innate lymphoid cells acquire memory-like properties and enhance allergic lung inflammation. *Immunity* 45:198–208.
41. Liu J, et al. (2013) Non-parallel recombination limits Cre-LoxP-based reporters as precise indicators of conditional genetic manipulation. *Genesis* 51:436–442.
42. Soriano P (1999) Generalized lacZ expression with the ROSA26 Cre reporter strain. *Nat Genet* 21:70–71.
43. National Research Council (2011) *Guide for the Care and Use of Laboratory Animals* (National Academies Press, Washington, DC), 8th Ed.
44. Font-Burgada J, et al. (2015) Hybrid periportal hepatocytes regenerate the injured liver without giving rise to cancer. *Cell* 162:766–779.